npj | flexible electronics

Article

Published in partnership with Nanjing Tech University

https://doi.org/10.1038/s41528-024-00331-1

Room temperature compressed air-stable conductive copper films for flexible electronics

H. Jessica Pereira [1,2] ✉, Oleg Makarovsky [3], David. B. Amabilino [4] & Graham N. Newton [1]

The state-of-the-art technology of fabricating printed copper electronics is focussed largely on thermal sintering restricting transition towards heat sensitive flexible substrates. Herein we report a pioneering technology which eliminates the need for conventional sintering. Biopolymer-stabilised copper particles are prepared such that they can be compressed at room temperature to generate air-stable films with very low resistivities (2.05 – 2.33 × 10^{-8} Ω m at 20 °C). A linear positive correlation of resistivity with temperature verifies excellent metallic character and electron microscopy confirms the formation of films with low porosity (< 4.6%). An aqueous ink formulation is used to fabricate conductive patterns on filter paper, first using a fountain/dip pen and then printing to deposit more defined patterns (R < 2 Ω). The remarkable conductivity and stability of the films, coupled with the sustainability of the approach could precipitate a paradigm-shift in the use of copper inks for printable electronics.

Copper (Cu) is an excellent electrical conductor, nearly matching the conductivity of silver (Cu: 5.96 × 10^7 S m^{-1} *vs* Ag: 6.30 × 10^7 S m^{-1}), but at a fraction of the cost (Cu: $ 0.28/oz *vs* Ag: $ 21.6/oz)[1] making it an ideal choice for cost-sensitive large-scale applications. Driven by the Internet of Things[2,3], most smart devices in the electronic industry require thin films of copper, with thicknesses in the nano or micrometre scale. These films are typically printed onto substrates from inks containing Cu particles (nano/microstructures) using techniques such as direct ink writing, doctor blading, screen/stencil printing or inkjet printing[4]. The deposited film subsequently undergoes sintering (thermal[5] or photon[6,7]), a process essential to facilitate solvent evaporation, decomposition of additives and binder molecules followed by inter-particle coalescence to form an interconnected network of Cu particles, resulting in an electrically conductive film[4,8]. Typically sintering is performed in an inert environment (N_2/Ar) or in a reducing atmosphere in the presence of H_2 or formic acid to mitigate the effects of inevitable oxidation induced by elevated temperatures, usually in the range of 200–350 °C[4,5]. The electrical conductivity achieved in each case is highly variable depending on the type of ink (nanoparticle, complex, salt, ion or hybrid), presence of stabilising agents, additives and binding agents, type of substrate (rigid or flexible) used for film formation, sintering temperatures and atmospheres. For thermally (250–275 °C) sintered films (vacuum, H_2 or formic acid), electrical resistivities in the range of 2.3[9]–92[10] μΩ cm have been reported in literature[5].

Despite the opportunities offered by Cu films, their use is particularly hindered by the propensity of Cu to oxidise in air. Research has focussed on surface passivation strategies to retard oxidation at the nano/microscale[11–14]. Organic ligands, particularly amines[15], carboxylic acids[16] and alkanethiols[17] have been used to stabilize Cu particles, because of their favourable interaction with the Cu surface. When forming films, however, extensive surface passivation of the Cu structures means that a high sintering temperature is necessary to achieve high electrical conductivity.

The rapid growth of the wearable and flexible electronics industry has motivated efforts to lower sintering temperatures (< 200 °C) or increase conductivities achieved at a given temperature, as most flexible substrates have low glass transition temperatures and undergo irreversible physical deformation at standard sintering temperatures[18]. Approaches include the incorporation of larger Cu particles or flakes[19], carbon nanotubes[20] and Cu salts[21] to the ink, and the use of smaller ligands[18,22] that allow electrons to tunnel between domains even when not completely decomposed. Another approach to lower the sintering temperature is to employ a Cu metal-organic decomposition ink in which the corresponding Cu precursor decomposes to form the metallic counterpart during the sintering

[1]The GSK Carbon Neutral Laboratories for Sustainable Chemistry, School of Chemistry, University of Nottingham, Nottingham, NG7 2TU, United Kingdom. [2]School of Electronics and Computer Science, University of Southampton, Southampton, SO17 1BJ, United Kingdom. [3]School of Physics, University of Nottingham, University Park, NG7 2RD, United Kingdom. [4]Institut de Ciència de Materials de Barcelona (ICMAB-CSIC), Consejo Superior de Investigaciones Científicas, Campus Universitari de Bellaterra, Cerdanyola del Vallès, 08193, Spain. ✉e-mail: H.J.Pereira@soton.ac.uk

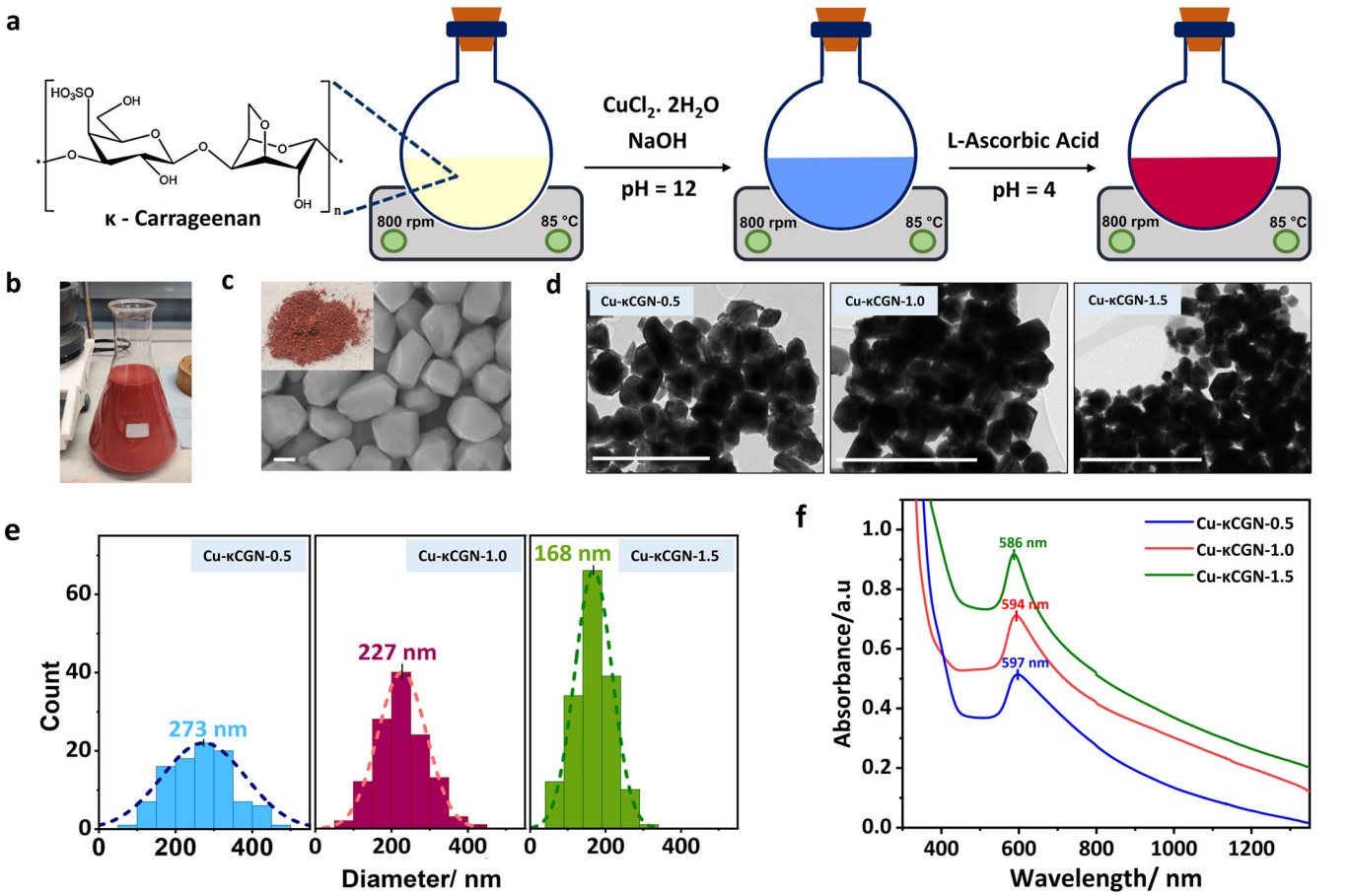

Fig. 1 | Synthesis and characterisation of Cu-κCGN particles. a Schematic representation showing the step-by-step synthesis of Cu-κCGN particles; **b** photograph showing the formation of a stable colloidal suspension; **c** a representative SEM image showing the shape of particles obtained in a typical synthesis. The scale corresponds to 100 nm. Inset in **c** is a photograph of the Cu-κCGN powder; **d** representative TEM images; and **e** corresponding particle size distributions for Cu-κCGN-0.5, Cu-κCGN-1.0 and Cu-κCGN-1.5 particles respectively. Particle size has been computed by measuring at least 100 particles for a given type. The scale corresponds to 1 μm; and **f** UV-Vis absorption spectra of Cu-κCGN samples showing the peak absorptions. The spectra corresponding to Cu-κCGN-0.5 and Cu-κCGN-1.0 have been offset along the y-axis for clarity.

process[4,5]. This approach has the advantage of limiting complications associated with oxidation of the metal as the ink usually consists of air-stable species such as Cu(II) formates, nitrates and sulfates or Cu oxides together with appropriate stabilising and reducing agents[23–25]. However, despite modest improvements, the state-of-the-art processing techniques still require sintering[4,5,8], which restricts substrate flexibility and expansion into more emerging areas such as flexible and paper-based electronics. A technology that supports the fabrication of conventional sintering-free Cu films without forfeiting their electronic properties would revolutionise the field of Cu-based electronics.

We set out to prepare stable aqueous suspensions of Cu particles that could form films with conductivities approaching that of the bulk metal without the need for thermal sintering. We hypothesised that this could be achieved using naturally occurring sulfated polysaccharides that could interact with the Cu particles[26–28] and introduce seaweed derived κ-carrageenan (κ-CGN), as an effective stabilising agent capable of providing stability without fully passivating the surface layer. We demonstrate that the particles prepared in this way can be compacted at room temperature to produce free-standing air-stable Cu films/discs that exhibit high electrical conductivity and a remarkably linear thermal response. Direct printing onto unmodified paper (and printed circuit board (PCB)) substrates have been demonstrated using simple ink deposition via a fountain pen as well as stencil printing. In all instances, SEM images clearly confirm the presence of films with excellent packing density and low porosity (< 4.6%). A Cu film prepared using our technology has been employed as the bottom electrode in fabricating an electroluminescent paper lamp to demonstrate potential scope of our approach. These films can potentially be fabricated on a range of substrates unlocking a diverse array of applications in the emerging field of paper electronics and flexible wearable electronics.

Results

Synthesis of Cu-κCGN particles and characterisation

The synthesis of sub-micron Cu particles uses κ-CGN, a biopolymer derived from red seaweed[29], as the stabilizing agent. Structurally, this biopolymer is a linear sulfated polysaccharide consisting of repeating β-d-galactose and 3,6-anhydro-α-d-galactose units (Fig. 1a) connected via α-(1,3) and β-(1,4) glycosidic linkages[30]. Here, κ-CGN was deemed suitable because it (i) is stable at basic pH values (no appreciable hydrolysis or degradation); (ii) bears hydroxyl and sulfate groups which can interact with the Cu(II) precursor forming a stable coordination complex[26]; (iii) is very inexpensive (£ 0.55-0.85 per gram); and (iv) is optically transparent.

The preparation of Cu particles (Cu-κCGN) is carried out in water under ambient atmospheric conditions as depicted in Fig. 1a. First the κ-CGN is dissolved at 85 °C, followed by addition of Cu(II) chloride dihydrate. Under these conditions, the divalent Cu precursor coordinates with κ-CGN via oxygen atoms in the sulfate and hydroxyl moieties[26,31]. The reaction mixture is then basified to pH 12

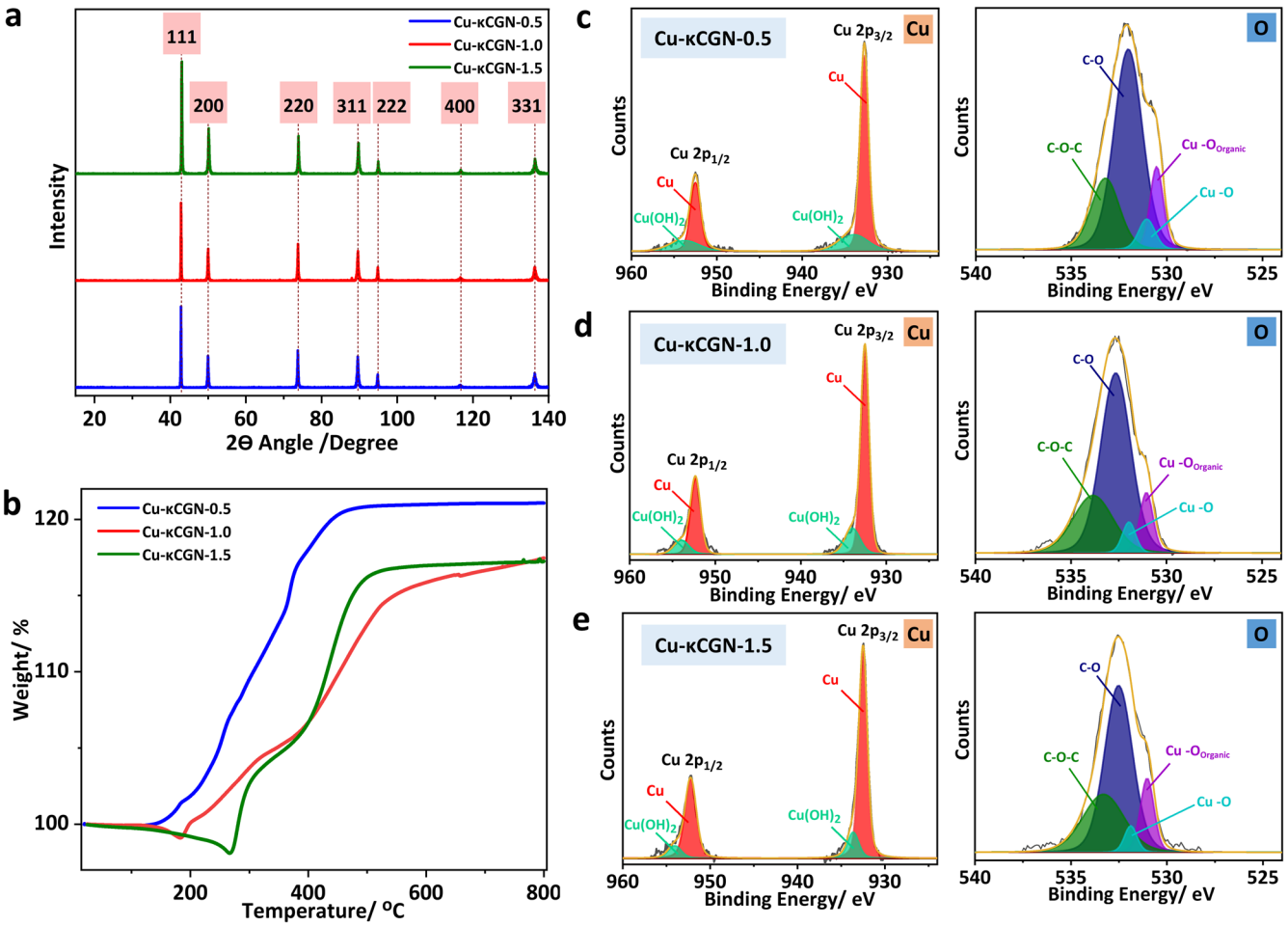

Fig. 2 | Thermal and ambient oxidative stability of Cu-κCGN particles. a PXRD patterns showing good agreement with the standard (ICSD – 43493) and good stability evident by the absence of peaks corresponding to oxides; **b** TGA analysis (in air) showing improved stability upon increasing the proportion of κ-CGN; and XPS analysis and corresponding peak assignments for Cu 2p and O 1 s core levels for the synthesised **c** Cu-κCGN-0.5, **d** Cu-κCGN-1.0 and **e** Cu-κCGN-1.5 powders showing that the samples predominantly consist of Cu(0). The PXRD patterns in **a** have been offset along the y axis for clarity.

(Supplementary Fig. 1). Subsequently, the Cu(II) precursor is reduced (Supplementary Fig. 2) by addition of L-ascorbic acid (vitamin C) to Cu(0), causing the solution to turn dark red (Fig. 1b and Supplementary Fig. 3). The as-synthesised Cu particles (concentration of 0.93 mg ml^{-1} per reaction) appear as a viscous reaction mixture with particles that are well-isolated from one another (Supplementary Fig. 4). As κ-CGN is a thermo-reversible gelling agent, upon cooling, the random κ-CGN coils undergo helical rearrangement[32] increasing the viscosity. The presence of well-isolated particles suggests that the κ-CGN helices partially passivate the Cu particles, preventing agglomeration. The isolated red-coloured powder (Fig.1c inset) consists of spherical particles as seen by the scanning electron micrograph (SEM) given in Fig. 1c.

The size and composition of the Cu-κCGN particles could be modulated by varying the loading of κ-CGN. Three Cu particle samples were prepared, identified as Cu-κCGN-0.5, Cu-κCGN-1.0 and Cu-κCGN-1.5 where the number signifies the amount of κ-CGN used as a percentage of weight by volume (i.e. 0.5% (w/v) of κ-CGN was added to Cu-κCGN-0.5). The amount of Cu(II) precursor is held constant, so that the relative proportion of κ-CGN to Cu(II) increases from Cu-κCGN-0.5 to Cu-κCGN-1.5. Representative transmission electron microscopy (TEM) images given in Fig. 1d and particle size distributions in Fig. 1e. show that the particles decrease in size as the amount of κ-CGN is increased. This observation was also supported by UV-Vis absorption spectroscopic analysis (Fig. 1f) which showed a blue shift in the plasmonic peak as the amount of κ-CGN increased. A synthesis in the absence of κ-CGN was also carried out as a control experiment. However, as evidenced by representative SEM images (Supplementary Fig. 5), the particles showed very poor uniformity in both size and shape, corroborating the important role of κ-CGN in controlling both these parameters.

Thermal and ambient oxidative stability of Cu-κCGN particles

Powder X-ray diffraction (PXRD) patterns collected for the Cu-κCGN particles were in good agreement with the standard face-centred cubic system observed for Cu (Fig. 2a and Supplementary Fig. 6). Notably, although all processing of the particles and PXRD were collected in air, there is no evidence of surface oxides and all peaks are of good intensity and align perfectly with the standard (ICSD – 43493), suggesting good stability in an ambient environment. Given the predisposition of Cu to oxidise when exposed to moisture and oxygen, particularly at elevated temperatures[33,34], thermogravimetric analysis (TGA) was used to assess the thermal stability under an oxygenated environment (Fig. 2b). An increase in weight over time was observed because of the gradual oxidation and the resulting formation of Cu_2O and CuO[35]. The stability of Cu particles is influenced by the amount of κ-CGN present in each Cu sample. κ-CGN acts as a protective barrier retarding the commencement of oxidation when the samples are heated in an

oxygenated environment as evidenced by the delayed on-set of aerobic oxidation. Cu-κCGN-0.5, Cu-κCGN-1.0 and Cu-κCGN-1.5 samples commence oxidation at 116, 183 and 266 °C respectively, indicating improved stability as the amount of capping ligand is gradually increased. Pristine κ-CGN begins decomposition at about 180 °C which is completed at 500 °C, leaving a residue of 20% which does not undergo further decomposition[36] (Supplementary Fig. 7). Therefore, as the temperature is gradually increased in an oxygenated environment with the decomposition of κ-CGN, surface Cu layers begin to oxidise resulting in an increase in weight. The sample with the lowest amount of κ-CGN undergoes rapid oxidation and reaches a maximum weight gain of 21%. The other two samples, which have higher amounts of κ-CGN begin oxidation at an elevated temperature (183 and 266 °C, respectively) and reach a weight gain of 17%. Consequently, the Cu-κCGN-0.5 sample shows an additional weight gain of 4% despite having slightly larger particles (and therefore a lower surface to volume ratio), indicating lowest stability of the 3 samples. The shape of the thermograms corresponding to Cu-κCGN-1.0 and Cu-κCGN-1.5 show two steps in oxidation; formation of Cu_2O and CuO, which is separated by a meta-stable state of oxidation, Cu_3O_4, observed at about 400 °C[37]. On the contrary, the Cu-κCGN-0.5 sample rapidly oxidises to Cu_2O and subsequently CuO. The metastable state is not evident for this sample. Additionally, the TGA data and elemental analysis (Supplementary Table 1) of the Cu-κCGN powders, both show that the amount of κ-CGN in each sample is very low (C < 1.5%) and therefore the observed thermal and ambient oxidative stability is impressive.

X-ray Photoelectron Spectroscopy (XPS) analysis was performed to further probe the surface stability of the Cu-κCGN powders as shown in Fig. 2c–e (and Supplementary Fig. 8). The presence of the characteristic Cu $2p_{3/2}$ (932.56 ± 0.05 eV) and Cu $2p_{1/2}$ (952.52 ± 0.05 eV) peaks confirm the presence of metallic Cu, which is also corroborated by Cu LMM Auger electron spectroscopy (Supplementary Fig. 9)[38]. Notably, apart from a small amount of $Cu(OH)_2$, which is likely to be a result of the strong base reacting with minute amounts of the metal precursor, all powders show very good stability under ambient conditions, with the highest stability for Cu-κCGN-1.5 as evident by more defined narrower Cu 2p peaks and a smaller peak for $Cu(OH)_2$ (also noticeable in the O 1 s region). In addition to the peaks corresponding to C-O-C and C-O, which originate from κ-CGN[39] (Supplementary Fig. 10), the O 1s XPS of all three types show an additional peak (530.27 ± 0.22 eV), which is absent in pure κ-CGN. A peak in this region has been designated to an interaction between an oxygen bonded to a carbon atom and transition metal elements[40,41]. Therefore, XPS analysis shows that κ-CGN stabilises the Cu by an interaction via oxygen atoms. A similar interaction, between the metal and oxygen atoms, is reported in the literature for κ-CGN capped gold[42] and silver[43] nanoparticles.

The XPS of the S 2p region showed relatively insignificant peak intensities (Supplementary Fig. 11). We speculate that the sulfate appendages are buried in, away from the surface and hence difficult to detect especially as there is only one such sulfate group per disaccharide unit. Matrix assisted laser desorption ionization time of flight mass spectrometry (MALDI-TOF MS) was carried out to test this hypothesis. The characteristic fragments corresponding to the 3-linked β-d-galactose (G-units) and 4-linked α-d-galactose (D-units) units of κ-CGN (Supplementary Fig. 12), are visible in the negative mode, confirming our postulation.

Film formation by compression

The as-synthesised particles (Fig. 3a) although not immediately conductive, when gently ground using a mortar and pestle, gradually transformed into a reflective layer (Fig. 3b), which was very conductive (Fig. 3c). This unexpected finding formed the basis for exploring a pressure treatment to generate conductive Cu films. Accordingly, the powder was transferred into a stainless-steel quick press die-set and compressed using a bench press (Fig. 3d and Supplementary Fig. 13). Preliminary measurements performed with a digital multimeter showed extremely low resistance verifying the excellent conductivity of these unsupported (i.e. with no underlying substrate) Cu films (Fig. 3e inset and Supplementary Fig. 13). This approach permits thickness modulation via the amount of powder used in the preparation and the force of compression. Shape modification can be achieved by simple customisation of the die-set. For subsequent characterisations, the film thickness was maintained between 25–30 μm for ease of handling (Supplementary Fig. 14).

Electrical properties and long-term stability of Cu films fabricated via room-temperature compression

The four-terminal resistance of the films fabricated from each of the three powders were measured (Supplementary Table 2) using the van der Pauw method[44]. All films show very low resistivities, with values for Cu-κCGN-0.5 and Cu-κCGN-1.0 approaching that of bulk Cu (1.69×10^{-8} Ω m or 5.96×10^7 S m^{-1}). For a metal film of this nature, the measured resistance is governed by additives and impurities (and their properties) as well as the microstructure (efficiency of packing)[4,45]. As κ-CGN itself is an insulator, higher loadings will undoubtedly contribute to increased resistance. However, in this context as loadings are not vastly different and the carbon percentage is low (Supplementary Table 1), the microstructure of the film, which is influenced by the particle size and distribution is likely to play a dominant role. To understand the influence of film microstructure and surface morphology on the measured electrical conductivity of the compressed Cu films, the porosity of representative SEM images, as a percentage of the total area of the image, was computed using ImageJ software (Supplementary Fig. 15). It is clear that the film made using Cu-κCGN-1.0 particles (Fig. 3e) is very compact with a negligible porosity of 1.76%, and accordingly shows the highest conductivity[46,47] ($4.53 \pm 0.51 \times 10^7$ S m^{-1}). Conversely, the film derived from the smallest particles (Cu-κCGN-1.5) shows the lowest conductivity ($0.67 \pm 0.95 \times 10^7$ S m^{-1}) because of the apparent high porosity of 9.03% arising from the inter-particle gaps (Fig. 3g). This is further impacted by the smaller grain size (i.e. smallest particles among the three samples) which contributes to an increased number of grain boundaries per unit area, generating a larger barrier for electron transport[48]. The electrical conductivity of the Cu-κCGN-0.5 film ($4.05 \pm 0.10 \times 10^7$ S m^{-1}) is only marginally lower than that of Cu-κCGN-1.0. This could be attributed to the presence of larger particles with a broader size distribution which has a favourable effect on the microstructure. The measured electrical conductivity is further influenced by the applied pressure (Supplementary Fig. 16 and 17), which dictates how well the particles are compressed.

Resistivity (ρ) of an ideal metallic film increases with temperature (T) due to increasing density of phonons in the lattice[49], in accordance with $\rho \sim \alpha T$, where α is the temperature coefficient of resistance. The opposite is true for granular films formed by weakly coupled metal particles[50,51], where electrical conductivity is limited by the tunnelling barriers formed between the particles, which become more transparent at high temperatures. Thus, direction and shape of the $\rho(T)$ dependence provides an excellent tool for probing the microscopic nature of electron transport in metal films. To probe the temperature dependence of resistivity of the fabricated films, four-terminal resistance was measured over a temperature range of 145 to 400 K (−130 to 130 °C). As shown in the graphs in Fig. 4a, the films composed of Cu-κCGN-0.5 and Cu-κCGN-1.0 show a remarkably linear relationship with temperature, similar to that of commercial Cu foil (Com-Cu-Foil, 99.8% metal content). Some nonlinearity is observed in the Cu-κCGN-1.5 sample, possibly due to resistance at the inter-particle barriers. This is not unexpected as this sample also showed the highest deviation from bulk Cu in respect to measured resistance. The corresponding α values (Supplementary Table 3) were calculated (α_{cal}) using the linear plot in Fig. 4a and Eq. 1[52]:

$$R = R_{ref}\left[1 + \alpha\left(T - T_{ref}\right)\right] \quad (1)$$

where R is the resistance at a given temperature T, and R_{ref} is the resistance at a given reference temperature T_{ref} for which the α value is calculated (20 °C for this work). All values deviate from the expected value for pure bulk

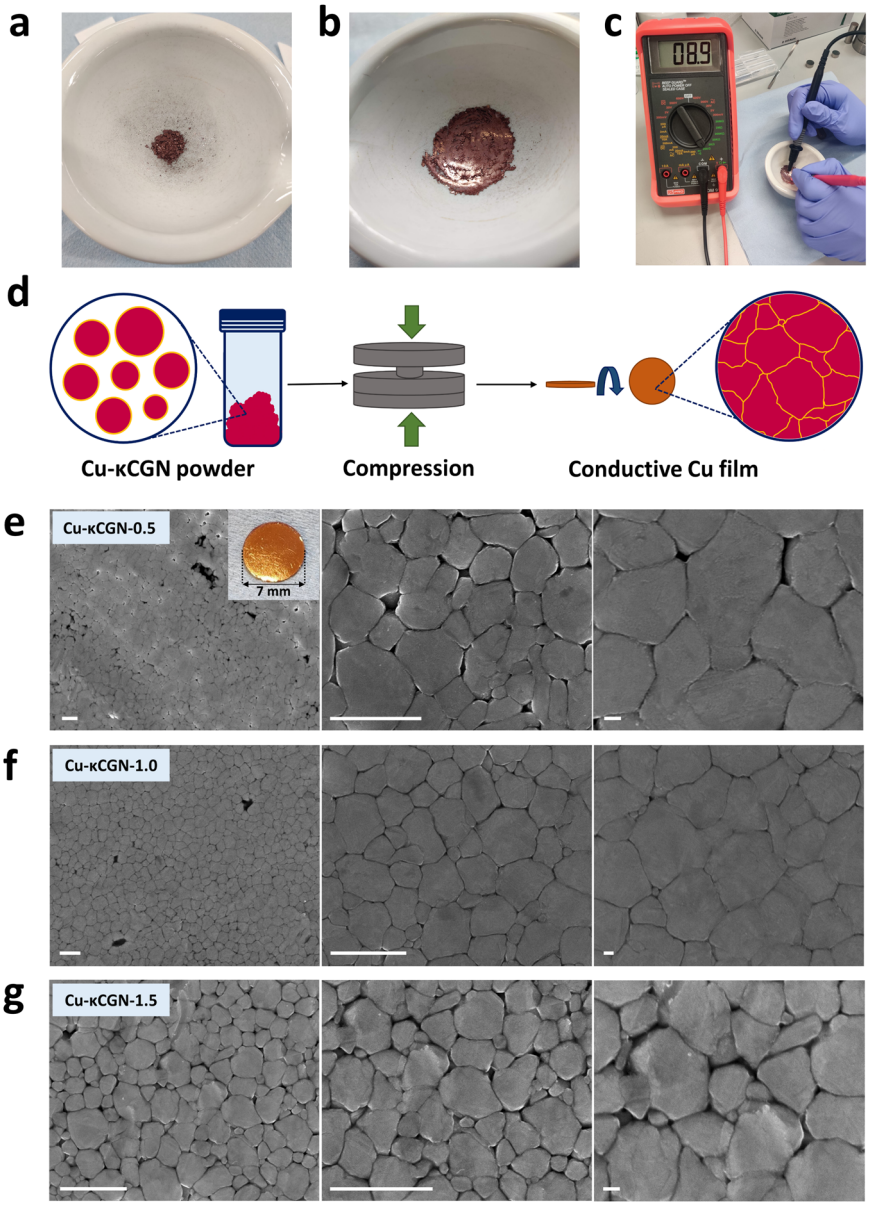

Fig. 3 | Film formation using room temperature compression and film morphology. Photographs showing **a** the dried Cu powder; **b** the formation of a lustrous film on the mortar upon gentle grinding of the powder; **c** a low resistance reading (8.9 Ω) on the multimeter confirming that the layer in **b** is very conductive; **d** schematic representation showing the compression process of Cu powders to fabricate Cu films; representative SEM images of increasing magnification (scale bars represent 1 μm, 1 μm and 100 nm respectively) showing the surface morphology of the films prepared using **e** Cu-κCGN-0.5; **f** Cu-κCGN-1.0 and **g** Cu-κCGN-1.5 powders. Inset in **e** shows a photograph of a typical Cu film prepared in this work.

Cu (0.00369 – 0.00409 °C^{-1} (at 20 °C))[52,53], as these are thin metal films and therefore affected by imperfections including vacancies, dislocations, foreign molecules and additives[54]. The trend however, illustrates that a decrease in particle size causes progressive reduction of α_{cal}. The organic content alone is far too low (Supplementary Table 1) to have a notable effect on α_{cal}. Thus, a far more plausible explanation, is the effect of grain boundaries. The higher the number of grain boundaries, the greater the deviation. Grain boundaries are defects in a polycrystalline material and are usually located at the interface between two crystallites. Although the crystal structure and the composition of the adjacent grains are identical, the change in orientation causes a planar defect, increasing electron scattering[48,55] which affects the electron-phonon interaction presented by the $\rho \sim \alpha T$ relation. Thus, larger particles generate a lower number of grain boundaries per unit area, compared to smaller particles[48,55] (Fig. 3e–g), consequently, the effect of grain boundaries become more pronounced for smaller particles[55]. A similar trend in α values has also been experimentally observed for gadolinium metal particles where the deviation was the highest for nanoparticles and lowest for microparticles[56]. A plot of resistivity vs temperature enables the deduction of resistivity of Cu-κCGN films at 20 °C; (ρ_{20}) (Fig. 4b and Supplementary Table 3). The corresponding α_{cal} and ρ_{20} values are summarised in Fig. 4c. Remarkably, the resistivity of these films (ρ_{20}) prepared via a conventional sintering-free room-temperature compression approach closely matches that of the bulk metal, with those of Cu-κCGN-1.0 and Cu-κCGN-0.5 only 1.22 and 1.38 times greater, respectively. The high conductivities obtained using our room temperature compression approach is enhanced by the oxidative stability of the particles, which retards formation of an outer oxide layer that could otherwise deplete film conductivity[57], and the formation of a smooth planar surface (Supplementary Fig. 18) which minimises unfavourable electron scattering caused by surface roughness[58].

Film formation via compression was done under ambient atmospheric conditions, therefore surface stability was evaluated using a further XPS analysis which shows (Supplementary Fig. 19 and 20) very similar data to that of corresponding isolated Cu powders, hence, excellent stability. Notably the compressed films show a more pronounced peak at 530.27 ± 0.22 eV indicating improved interaction between Cu and κ-CGN when compressed (Insets in Supplementary Fig. 19). The long-term stability was further assessed by leaving the Cu-κCGN-1.0 film (best-performing sample) under ambient conditions for 7.5 months followed by a subsequent XPS analysis. As presented in Fig. 4d (and Supplementary Fig. 21), the

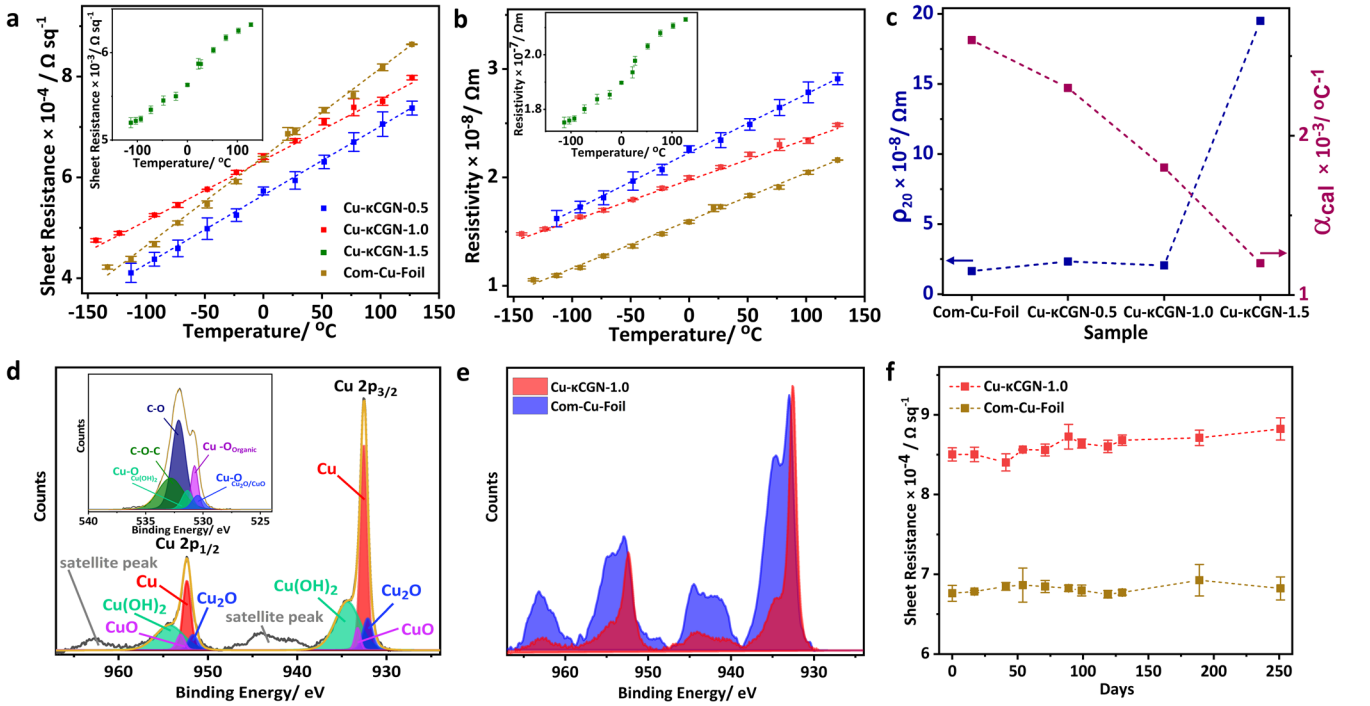

Fig. 4 | Electrical properties and long-term stability of films prepared via compression. a Four-terminal sheet resistance vs temperature measurements; **b** resistivity vs temperature measurements for films prepared using Cu-κCGN-0.5, Cu-κCGN-1.0, and Com-Cu-Foil. Inset in **a** shows four-terminal sheet resistance vs temperature measurements for films prepared using Cu-κCGN-1.5 powder. Inset in **b** shows the resistivity vs temperature measurements for films prepared using Cu-κCGN-1.5 powder. (graphs in **a** and **b** are fitted using Eq. 1 with corresponding α_{cal} values shown in **c**); **c** Comparison of measured resistivities (at 20 °C) and temperature coefficient of resistance of each Cu film; **d** XPS analysis and peak assignments for Cu 2p core levels for Cu films prepared using the Cu-κCGN-1.0 powder, left under ambient atmospheric conditions for 7.5 months. Inset in **d** shows XPS analysis and corresponding peak assignments for O 1s core levels; **e** overlay of **d** and XPS analysis of Cu 2p core levels for a similarly exposed Com-Cu-Foil sample; and **f** long-term four-terminal sheet resistance measurements for Cu films prepared using Cu-κCGN-1.0 powder and Com-Cu-Foil. The error bars represent +/- standard deviation for at least two four-terminal resistance measurements, performed according to the van der Pauw method.

stability of the film is significantly better compared to a similarly exposed Com-Cu-Foil sample (Fig. 4e). The latter shows prominent satellite peaks indicating the presence of Cu(II) species, hence, surface oxidation[38]. The four-terminal sheet resistance was also monitored over time and shows (Fig. 4f and Supplementary Fig. 22) excellent stability over 250 days, with only a 4% increase in resistance. All films fabricated with the current formulation are highly reflective and show very good resemblance to that typically observed for metallic Cu (Supplementary Fig. 23), with high reflectivity up to a wavelength (λ) ≥ 600 nm, which then decreases gradually at λ < 550 nm because of inter-band transition energy losses[59,60]. Formation of a continuous passivation layer is implausible as the carbon content is low (Supplementary Table 1). However, the films show appreciable stability. We postulate that this is a result of the supramolecular arrangement of κ-CGN helices which accumulate at the interparticle gaps, i.e. at the grain boundaries, when compressed under high pressure, passivating these sites which are most susceptible to oxidation[61]. Additionally, when compressed under high pressure, particles are forced into place, rather than the gradual coalescence observed in conventional sintering, enabling controlled densification, minimizing interparticle gaps and pores, thereby restricting ingress and lateral diffusion of oxygen.

Fabrication of films on paper and PCB substrates

To demonstrate the practicality of our conventional sintering-free approach, Cu patterns were drawn on filter paper using an ink formulation. The particles were suspended in deionized water together with L-ascorbic acid (15 mM) as an antioxidant[18,57] (Fig. 5a) followed by ink deposition using a fountain pen (or a calligraphy dip pen). The deposited pattern was subsequently dried under vacuum to completely remove the solvent and pressed to form a highly reflective and conductive paper electrode as seen in Fig. 5b–d. These paper electrodes are flexible and can be subjected to physical deformation without film delamination. The optical microscope and SEM images in Fig. 5e and f, show that the Cu particles pack densely in between the randomly distributed cellulose fibres, giving rise to an interconnected compact layer of Cu (Fig. 5g). All patterns are deposited on unmodified filter paper, thus, there is potential for further improvement via appropriate surface pre-treatments[62,63]. We also demonstrate successful patterning on PCB substrates using this technology (Fig. 5h). Conventionally, PCB circuits are made by depositing a layer of Cu followed by lithography/masking and etching to remove the unwanted coverage resulting in a circuit of a desired pattern. A combination of etching and plating techniques serves as the mainstream fabrication method with appropriate modifications in microfabrication and processing to achieve finer traces[64,65]. For this work, the PCB substrate was UV/O_3 treated to improve surface hydrophilicity, prior to ink deposition. Remarkably, the resulting print was very smooth and highly reflective with very low resistance (Fig. 5i) owing to the presence of a dense layer of well-connected Cu particles (Fig. 5j, k).

Printing conductive Cu patterns on paper and fabrication of an electroluminescent paper lamp

To demonstrate that the existing ink formulation can be used in combination with standard printing technology often used to deposit such materials in the field, we employed a printing approach that utilises a stainless-steel stencil to transfer patterns on to filter paper. As shown by the results illustrated in Fig. 6a and b, Cu patterns were successfully transferred on to the underlying filter paper (unmodified) and show very good conductivity as evidenced by the low resistance readings depicted in the corresponding photographs given in Fig. 6c–f. The latter also shows good

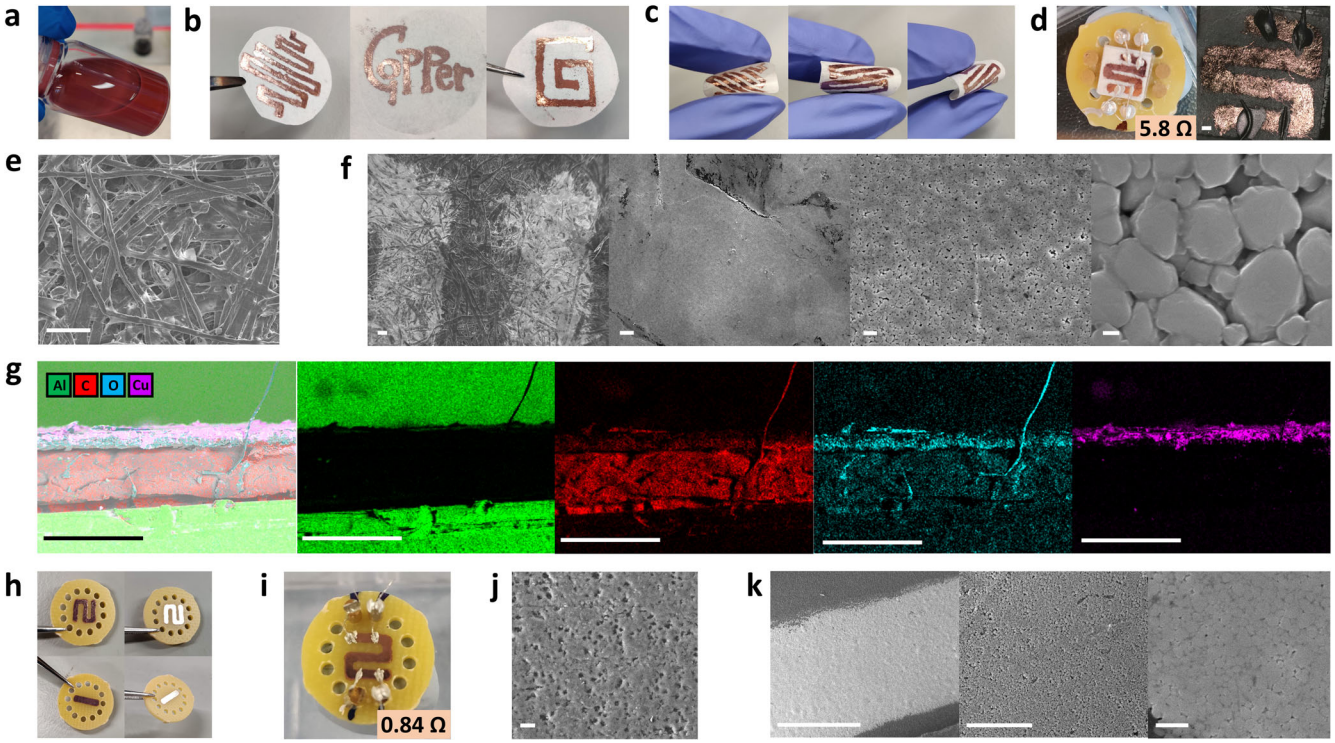

Fig. 5 | Fabrication of Cu films on paper and PCB substrates. Photographs showing **a** the Cu ink used to prepare patterned electrodes on paper and PCB substrates; **b** various Cu patterns on filter paper; **c** physical deformation of an electrode on filter paper - no delamination of the Cu film occurs upon bending; **d** a typical sample used for four-terminal electrical measurements of films on paper and the corresponding optical micrograph (scale bar corresponds to 200 µm); SEM images of **e** filter paper (scale bar corresponds to 100 µm); and **f** Cu films on filter paper (of increasing magnification with scale bars representing 100 µm, 10 µm, 1 µm and 100 nm respectively); **g** cross sectional EDXS analysis of a Cu film on paper showing the overlayed image and elemental composition (scale bars correspond to 500 µm): Al (from the SEM stub), C, O and Cu; Photographs showing **h** smooth and highly reflective Cu patterns on PCB substrates; **i** a typical sample used for four-terminal electrical measurements of films on PCB substrates; SEM images of **j** the PCB substrate (scale bar corresponds to 10 µm); and **k** Cu films on PCB substrates (of increasing magnification with scale bars representing 1 mm, 10 µm and 1 µm respectively).

sensitivity to pattern length with gradual increase in measured resistance (from pattern 1 to 4) as the length of the pattern is increased. Although some edge defects and discontinuity in the transferred ink pattern (Supplementary Fig. 24) can be observed in a few prints, all continuous patterns are conductive (Supplementary Fig. 24). It is important to note that this is a mere demonstration to show that printing can be done, and further optimisation is necessary (including surface modification of the paper substrates to limit spreading of the ink, ink viscosity adjustments, concentration/loading optimisation) and will support in perfecting the print. Although further optimisation is necessary, the results are conclusive proof-of-concept, demonstrating the ease and efficiency with which paper electrodes can be prepared using this approach. These electrodes are potentially the basis for developing paper-based electronic devices which is not feasible with conventional heat-based sintering. We foresee that the development of the technology will require additional electrical and surface understanding to gain insight into surface and interfacial chemistry of Cu films prepared using this technology to facilitate device design.

To demonstrate the flexibility of the printed Cu patterns on paper, a bending test was performed using the setup reported by Komolafe et al.[66] (Supplementary Fig. 25) in which a printed Cu film on paper (1 mm × 7 mm, Fig. 6g**:** inset) was subjected to 1000 bending cycles along two bending radii; 10 mm and 5 mm. As shown in Fig. 6g, an increase in the relative resistance (R/R_0) is observed for both bending radii with a R/R_0 of 1.6 and 5.7 for 10 mm and 5 mm, respectively. A smaller radius is expected to have a larger impact on the R/R_0 value, in accordance with similar observations in literature[67,68], as a smaller radius impacts the strain on the substrate and film to a greater extent[69]. To maintain the current system as sustainable as possible, we wished to avoid modification of the paper substrate or encapsulation, or film passivation used in other systems to improve rigidity. Hence, the relative increase in resistance is appreciable.

Although Cu films have been previously printed on various flexible substrates, in respect to cellulose/paper, most reports focus on a copper-cellulose composite where cellulose serves as a matrix material[70–72]. The presence of cellulose in larger proportions as well as existence of both copper and copper oxides makes it difficult to achieve high electrical conductivities. However, in this work, the development of a compression-based approach to fabricate copper films have proven to be successful in realising films with excellent electrical conductivity ($2.05 - 2.33 \times 10^{-8}$ Ω m at 20 °C) and high metallic character without the need for sophisticated sintering techniques and inert or reducing atmospheres[5]. Our approach is relatively simple and greener, supporting sustainable chemistry and processing.

To demonstrate that a Cu electrode developed using our compression approach can be used to fabricate electronic devices, we fabricated an electroluminescent paper lamp as proof-of-concept. The lamp was based on a typical capacitor architecture that utilised a compressed Cu electrode as the bottom contact. The subsequent layers in order of deposition include a dielectric layer to prevent short-circuiting and to promote light reflection, a phosphor layer consisting of doped zinc sulfide which emits light in response to an applied electric field, a silver electrode to facilitate uniform charge distribution and a top PEDOT:PSS transparent electrode to allow light transmission[73,74] (Fig. 6h and Supplementary Fig. 26). The Cu base layer was printed (stencil) and processed using our standard room temperature compression protocol. The subsequent layers were deposited via printing and cured for 10 min each at 120 °C in a vacuum oven. As evidenced by the photograph given in Fig. 6i (and Supplementary Fig. 26), the electroluminescent effect can be clearly observed upon applying an

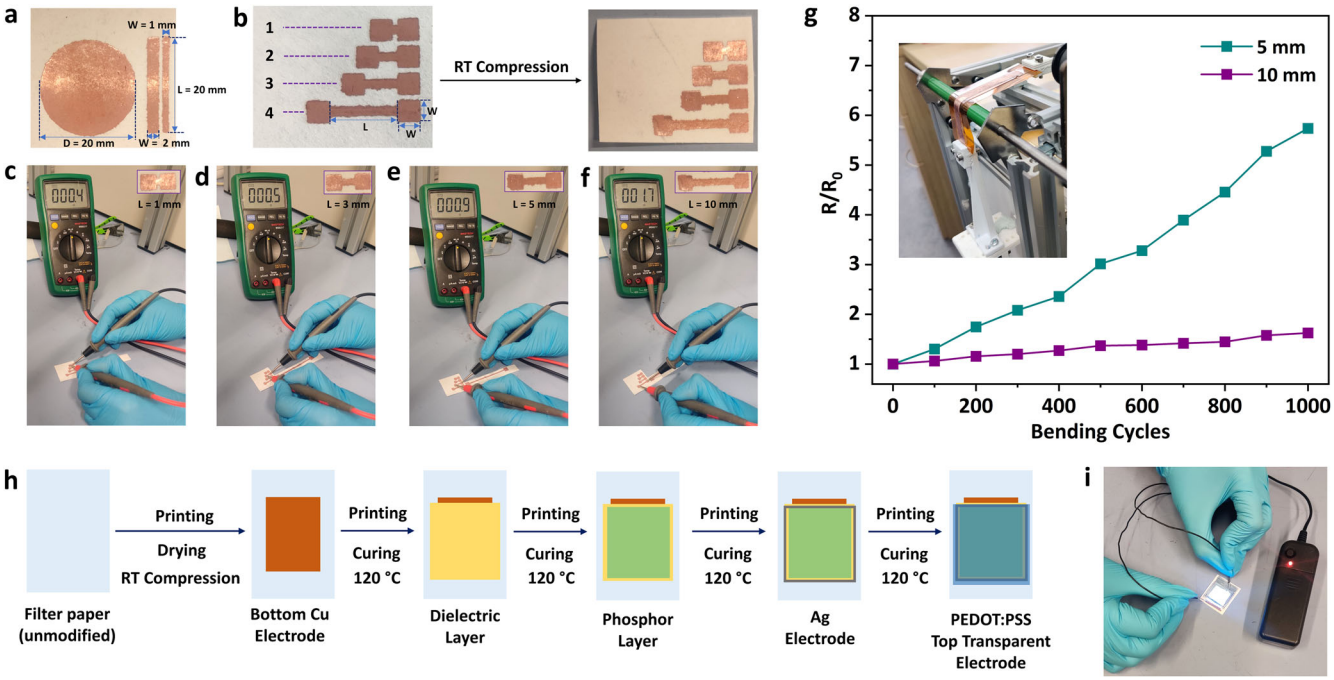

Fig. 6 | Printing conductive Cu patterns on paper and fabrication of an electroluminescent paper lamp. Photographs showing **a** a typical stencil printed Cu pattern; **b** the printed patterns on filter paper before and after compression; a measured low resistance (< 2 Ω) corresponding to individual patterns denoted by **c** 1; **d** 2; **e** 3; and **f** 4, following compression. Insets of **c** – **f** show the specific pattern of which the resistance is measured and the corresponding dimensions. In all patterns given in **c** – **f**, W = 3 mm; **g** a plot of R/R_0 vs bending cycles showing the relative change in resistance when a printed Cu film on a paper substrate is subjected to 1000 bending cycles with a bending radius of 10 mm and 5 mm respectively. Inset in **g** shows a photograph which depicts a Cu film being subjected to bending in the test set up; **h** a schematic showing the step-by-step fabrication process of an electroluminescent paper lamp which uses a compressed Cu film on unmodified filter paper as the bottom electrode and **i** a photograph showing the light emission from the paper based electroluminescent device in response to an electric field. Unmodified filter paper was used as the substrate for all patterns and the printing was done using an ink consisting of Cu-κCGN-1.0 particles.

alternating electric field. Successful fabrication and demonstration of a proof-of-concept device based on our compressed Cu electrode material illustrates the potential scope of applications of our system.

Discussion

We demonstrate a different approach to the fabrication of highly conductive Cu films based on the room temperature compression of κ-CGN stabilised Cu particles. Three types of Cu particles have been synthesised, Cu-κCGN-0.5, Cu-κCGN-1.0 and Cu-κCGN-1.5, by varying the loading of κ-CGN. The particles are of sub-micron range and size can be tuned by modulating the amount of κ-CGN and this proportion also has an impact on the stability of the resultant Cu powders. The isolated powders can be compressed at room temperature to fabricate unsupported copper films with conductivities close to those of the bulk metal in the absence of any heat treatment. SEM images show that the particles are densely packed in the films, forming a well-connected network of compressed particles with a very smooth surface which minimizes scattering and enhances electron transport. The successful transfer of the process to paper and PCB substrates and the excellent conductivity, flexibility and mechanical stability of the films formed demonstrates the broad applicability of this approach. Combining the conductivity and oxidative stability of the copper films, with the low energy synthesis of the particles from renewable resources and the ease with which films can be formed on a range of substrates, this system has the potential to open new doors in the use of copper inks for printable electronics.

Methods

Materials

Copper(II) chloride dihydrate ($CuCl_2.2H_2O$, 99%, Fisher Scientific), Kappa carrageenan (sulfated plant polysaccharide, Sigma-Aldrich), L-ascorbic acid (99 + %, Alfa Aesar), sodium hydroxide (99 + %, Alfa Aesar), disposable polypropylene centrifuge tubes (50 ml, Fisher Scientific), IPA (99.5%, Fisher chemical) and acetone. The materials and solvents were used as received without further purification.

Synthesis of copper particles

An aqueous solution of κ-CGN was prepared by dissolving κ-CGN (0.6 g, 0.5% w/v) in 120 ml of deionised water at a temperature of 85 °C and stirred at 800 rpm. Upon complete dissolution, $CuCl_2.2H_2O$ (2.37 mmol, 0.02 M) was added to the reaction flask. Subsequently, the reaction mixture was basified to a pH of 12 using a NaOH (2.7 M) solution. Then the reducing agent, L-ascorbic acid (2.0 M, 10 ml) was added until a pH of 4-5 was reached upon which the blue solution turns yellow, white, and finally red. The appearance of red colour takes about 15 min. The reaction was maintained at 85 °C and stirred at 800 rpm for 5 h and then cooled down to room temperature. The particles were isolated by centrifuging at 8000 rpm for 15 min using a Thermo Scientific Heraeus Megafuge 8 centrifuge. Each reaction (total volume about 135 ml) yields 126 ± 5.8 mg of the Cu-κCGN particles. Therefore, the concentration of Cu per reaction is 0.93 mg ml^{-1}. The solid particles were then repeatedly washed with deionised water and dried under vacuum to isolate the particles in the form of a red powder. (All experiments were performed under ambient conditions, unless otherwise stated).

Fabrication of free-standing films

The dried Cu particles were ground to a fine powder using a mortar and pestle and transferred (30 mg) to a quick press-die set (circular in shape with a diameter of 7 mm) and then a load was applied using the hydraulic bench press (See Supplementary Fig. 13 and Supplementary Note 17). The pressure was varied from 2.44×10^2 – 1.22×10^3 bar, to study the effect on film formation and resulting conductivity. Commercially available Cu foil (Com-Cu-Foil, 99.8% metal basis) of similar thickness (25 µm) was chosen as a suitable candidate for comparison, to benchmark our films as it is widely used for diverse electrical applications. Attempts to fabricate similar unsupported Cu films using commercially available metallic Cu powders were proven unsuccessful.

Fabrication of conductive patterns on paper and PCB substrates

The Cu ink was formed by suspending the Cu particles in deionized water (60–70 mg ml^{-1}) together with L-ascorbic acid (15 mM) as an antioxidant, followed by sonication (5 min). The contact angle and surface tension of the Cu ink was 38.4° and 59.2 mN m^{-1} respectively (Supplementary Fig. 27). The ink was then deposited using a fountain pen or a calligraphy dip pen (for improved control over line thickness). For paper substrates no pre-treatment was done. For PCB substrates, UV/O_3 treatment (10 min) was done prior to deposition. Subsequently, the deposited pattern was dried under vacuum and compressed (2.44 – 6.10×10^2 bar) using a hydraulic bench press to realise a conductive Cu pattern. For printing, a stainless-steel laser cut stencil (MCI precision screens Ltd) was used, and the ink was transferred on to the underlying filter paper using a squeegee.

Resistance measurements using four-terminal van der Pauw and collinear methods

The van der Pauw method was deemed suitable to measure the sheet resistance and deduce the electrical conductivity of compressed free-standing copper films of thickness in the range of 25–30 µm. As shown by SEM images the samples are adequately homogenous and exhibit low porosity. However, prior to measuring our own samples, to validate our experimental set up, we first measured the electrical conductivity of commercially purchased Cu foil (99.8% metal basis, 1.673 µΩ cm at 20 °C). The van der Pauw method, measurement set up in our laboratory and relevant calculations provided an average electrical resistivity of 1.69×10^{-8} Ω m (or 1.69 µΩ cm) for commercial copper foil which is in good agreement with the provided value.

The pressed free-standing Cu films were cut to a square shape (5×5 mm^2) using a scalpel and loaded onto non-magnetic headers and fixed in place at the centre using double-sided tape. Four-contacts were made from each edge of the sample to the gold coated probes using silver paint (RS Pro conductive paint). Current-voltage dependences were measured using a Keithley-2400 sourcemeter and a Keithley-2010 multimeter. Four different current and potential contact configurations were carried out for each sample and processed using the van der Pauw technique. For temperature dependent resistance measurements, the headers were loaded onto a vacuum cryostat with temperature controlled in the range of 100 K < T < 500 K. The temperature in the liquid nitrogen cooled cryostat was changed as required in the range of −150 °C to 150 °C, using a Lake Shore Cryotronics (model 335) temperature controller. During all the measurements, low pressure in the cryostat was maintained by the vacuum pump (Pfeiffer Hi CUBE) at a level of $< 1 \times 10^{-4}$ hPa. For Cu patterns deposited on paper (Fig. 5d) and PCB (Fig. 5i) substrates, sample homogeneity, substrate porosity and surface roughness can limit the accuracy of van der Pauw measurements, hence the collinear 4-point probe method was used to measure the resistance of these samples. Four contacts, which cross the entire width of the sample were made on each long bar or snake-patterned sample, using silver paint and silver wires. The potential across the sample was measured using the inner two contacts and the resistance was calculated in accordance with the collinear technique.

Characterisation

The morphology of the particles was studied using a JEOL 2100 F TEM operating at 200 kV equipped with a Gatan Orius CCD camera and JEOL scanning transmission electron microscopy (STEM) detectors. ImageJ software was used to analyse the TEM images and compute particle size distributions. SAED patterns were also acquired with the Gatan Orius CCD camera. Calibration was done using an evaporated aluminium film as a reference (from Agar Scientific). Optical microscopy images (Cu particles in suspension, Cu films, Cu patterns on paper and PCB substrates) were collected using an Olympus BX51 Microscope in reflection mode unless otherwise specified. UV-Vis-NIR absorption spectra of aqueous Cu suspensions were obtained in the wavelength range of 300 nm to 1400 nm using an Agilent Cary UV-Vis-NIR spectrophotometer. For the current work, UV-Vis absorption spectroscopy was adopted to identify the presence of metallic copper and obtain a preliminary understanding regarding particle size, distribution and degree of agglomeration in various samples prior to conducting other more specific characterisation techniques such as TEM, SEM and XPS. TGA was performed (in air) using a TA instruments Discovery TGA with 100 µl Platinum-HT sample pans. PXRD measurements were collected using a Panalytical materials research diffractometer. The Cu particles were finely ground prior to loading onto the sample holder. Loading of samples and data acquisition was performed in air. The PXRD peaks were assigned using the Mercury software and the CDS National Chemical Database (ICSD – 43493). For SEM imaging a small sample of Cu (powder, free-standing film and patterns coated on substrates) was placed on the aluminium stub using adhesive carbon tape and imaging was performed using a JEOL 7100 Field Emission Scanning Electron Microscope with an accelerating voltage of 15 kV. For Cu particles in the form of a powder, iridium (8 nm) was coated prior to imaging. Coating of iridium was also done for samples on paper and PCB substrates to avoid background charging caused by non-conductive substrates. For Cu patterns on paper substrates, Energy-dispersive X-ray spectroscopy (EDXS) was acquired using an Oxford Instruments Ultim®Max-100 detector and processed with Oxford Instruments Aztec software. XPS (particles and free-standing films) was performed using the Kratos AXIS ULTRA with a monochromated Al Kα X-ray source (1486.6 eV) operated at 10 mA emission current and 12 kV anode potential (120 W). Spectra were acquired with the Kratos VISION II software. A charge neutralizer filament was used to prevent surface charging. Hybrid–slot mode was used for measuring a sample area of approximately 300 ×700 µm. The analysis chamber pressure was 5×10^{-9} mbar. Three areas per sample were analysed. A wide scan was performed at low resolution (binding energy range 1400 eV to −5 eV, with pass energy 80 eV, step 0.5 eV, sweep time 20 min). High resolution spectra at pass energy of 20 eV, step of 0.1 eV, and sweep time of 10 min each were also acquired for photoelectron peaks from the detected elements, and these were used to model the chemical composition. Sample loading to the XPS was performed in air. The spectra were charge corrected by setting the C 1s peak to 284.7 eV. Data analysis and processing was done using CasaXPS software. MALDI-TOF-MS data was collected using a Bruker Autoflex Max MALDI-TOF spectrometer. Samples were prepared by mixing the Cu particles (Cu-κCGN-1.5) with the matrix (DCTB: *trans*-2-[3-(4-*tert*-Butylphenyl)-2-methyl-2-propenylidene]malononitrile) in an Eppendorf tube followed by addition of deionised water. This was then mixed rigorously using a vortex mixer and spotted on a polished steel plate for analysis. Bending tests were performed using a printed Cu film (on unmodified filter paper) of dimensions 1 cm × 7 cm, and testing was performed along two bending radii; 5 mm and 10 mm, using the setup reported by Komolafe et al.[66] The set up consist of a cylindrical mandrel (which can be changed depending on the required bending radius) across which the sample is clamped in place via two sample holders (Supplementary Fig. 25). The movement of the sample is controlled by a motor. The latter is programmed using the Arduino software. A Kruss DSA30 drop shape analyser was used to measure the contact angle and surface tension of the Cu ink. To compute the surface tension, the images acquired by the drop shape analyser were

processed using ImageJ software with the pendent drop analysis plug-in reported by Daerr et al.[75].

Fabrication of an electroluminescent paper lamp

A Cu film was printed on unmodified filter paper, dried under vacuum, and compressed to obtain a conductive film. Subsequent ink layers consisting of particles and polymer binders (smart fabric ink Ltd) were then deposited via stencil printing and each layer was cured at 120 °C for 10 min in a vacuum oven. These include a dielectric layer (barium titanate, TC-C9001), a phosphor layer consisting of doped zinc sulfide (TC-P0001), a silver electrode (TC-C4001), and a top PEDOT: PSS transparent electrode (TC-C4006).

Data availability

The data that support the plots in this paper and other findings of this study are available from the corresponding author upon reasonable request.

Received: 14 December 2023; Accepted: 19 July 2024;
Published online: 27 July 2024

References

1. Haynes, W. M. (Ed.). *CRC Handbook of Chemistry and Physics 97th Edn*, (CRC Press, 2016).
2. Buga, C. S. & Viana, J. C. The role of printed electronics and related technologies in the development of smart connected products. *Flex. Print. Electron.* **7**, 043001 (2022).
3. Wiklund, J. et al. A review on printed electronics: Fabrication methods, inks, substrates, applications and environmental impacts. *J. Manuf. Mater. Process.* **5**, 89 (2021).
4. Zeng, X. et al. Copper inks for printed electronics: a review. *Nanoscale* **14**, 16003–16032 (2022).
5. Li, W. et al. The rise of conductive copper inks: challenges and perspectives. *Appl. Mater. Today* **18**, 100451 (2020).
6. Jung, J. et al. Moiré-Free Imperceptible and Flexible Random Metal Grid Electrodes with Large Figure-of-Merit by Photonic Sintering Control of Copper Nanoparticles. *ACS Appl. Mater. Interfaces* **11**, 15773–15780 (2019).
7. Jang, Y. R. et al. A Review on Intense Pulsed Light Sintering Technologies for Conductive Electrodes in Printed Electronics. *Int. J. Precis. Eng. Manuf. - Green. Technol.* **8**, 327–363 (2021).
8. Cano-Raya, C., Denchev, Z. Z., Cruz, S. F. & Viana, J. C. Chemistry of solid metal-based inks and pastes for printed electronics – A review. *Appl. Mater. Today* **15**, 416–430 (2019).
9. Woo, K., Kim, Y., Lee, B., Kim, J. & Moon, J. Effect of carboxylic acid on sintering of inkjet-printed copper nanoparticulate films. *ACS Appl. Mater. Interfaces* **3**, 2377–2382 (2011).
10. Jeong, S. et al. Controlling the thickness of the surface oxide layer on Cu nanoparticles for the fabrication of conductive structures by ink-jet printing. *Adv. Funct. Mater.* **18**, 679–686 (2008).
11. Stewart, I. E., Ye, S., Chen, Z., Flowers, P. F. & Wiley, B. J. Synthesis of Cu-Ag, Cu-Au, and Cu-Pt Core-Shell Nanowires and Their Use in Transparent Conducting Films. *Chem. Mater.* **27**, 7788–7794 (2015).
12. Kim, T. G. et al. Enhanced Oxidation-Resistant Cu@Ni Core-Shell Nanoparticles for Printed Flexible Electrodes. *ACS Appl. Mater. Interfaces* **10**, 1059–1066 (2018).
13. Jeong, G. et al. A highly robust and stable graphene-encapsulated Cu-grid hybrid transparent electrode demonstrating superior performance in organic solar cells. *J. Mater. Chem. A* **6**, 24805–24813 (2018).
14. Chen, Z., Ye, S., Stewart, I. E. & Wiley, B. J. Copper nanowire networks with transparent oxide shells that prevent oxidation without reducing transmittance. *ACS Nano* **8**, 9673–9679 (2014).
15. Cure, J. et al. Remarkable Decrease in the Oxidation Rate of Cu Nanocrystals Controlled by Alkylamine. *Ligands J. Phys. Chem. C.* **121**, 5253–5260 (2017).
16. Tokura, R., Tsukamoto, H., Tokunaga, T., Nguyen, M. T. & Yonezawa, T. The role of surface oxides and stabilising carboxylic acids of copper nanoparticles during low-temperature sintering. *Mater. Adv.* **3**, 4802–4812 (2022).
17. Dabera, G. et al. Retarding oxidation of copper nanoparticles without electrical isolation and the size dependence of work function. *Nat. Commun.* **8**, 1894 (2017).
18. Pereira, H. J., Killalea, C. E., & Amabilino, D. B. Low-Temperature Sintering of L-Alanine-Functionalized Metallic Copper Particles Affording Conductive Films with Excellent Oxidative Stability. *ACS Appl. Electron. Mater.* **4**, 2502–2515 (2022).
19. Lai, H., Wen, J., Yang, G., Zhang, Y. & Cu, C. Mixed Cu Nanoparticles and Cu Microparticles with Promising Low-temperature and Low-pressure Sintering Properties and Inoxidizability for Microelectronic Packaging Applications. in *2021 22nd International Conference on Electronic Packaging Technology, ICEPT 2021* (Institute of Electrical and Electronics Engineers Inc., 2021). https://doi.org/10.1109/ICEPT52650.2021.9568089.
20. Seong, K. et al. An Ultradurable and Uniform Cu Electrode by Blending Carbon Nanotube Fillers in Copper-Based Metal-Organic Decomposition Ink for Flexible Printed Electronics. *Adv. Mater. Interfaces* **5**, 1800502 (2018).
21. Yong, Y. et al. Effect of decomposition and organic residues on resistivity of copper films fabricated via low-temperature sintering of complex particle mixed dispersions. *Sci. Rep.* **7**, 1–9 (2017).
22. Kanzaki, M., Kawaguchi, Y. & Kawasaki, H. Fabrication of Conductive Copper Films on Flexible Polymer Substrates by Low-Temperature Sintering of Composite Cu Ink in Air. *ACS Appl. Mater. Interfaces* **9**, 20852–20858 (2017).
23. Kim, S. J., Lee, J., Choi, Y. H., Yeon, D. H. & Byun, Y. Effect of copper concentration in printable copper inks on film fabrication. *Thin Solid Films* **520**, 2731–2734 (2012).
24. Choi, Y. H. & Hong, S. H. Effect of the Amine Concentration on Phase Evolution and Densification in Printed Films Using Cu(II) Complex Ink. *Langmuir* **31**, 8101–8110 (2015).
25. Dai, X., Zhang, T., Shi, H., Zhang, Y. & Wang, T. Reactive Sintering of Cu Nanoparticles at Ambient Conditions for Printed Electronics. *ACS Omega* **5**, 13416–13423 (2020).
26. You, J. et al. Optical Detection of Copper Ions via Structural Dissociation of Plasmonic Sugar Nanoprobes. *Anal. Chem.* **94**, 5521–5529 (2022).
27. Jones, F., Cölfen, H. & Antonietti, M. Interaction of κ-carrageenan with nickel, cobalt, and iron hydroxides. *Biomacromolecules* **1**, 556–563 (2000).
28. Jones, F., Cölfen, H. & Antonietti, M. Iron oxyhydroxide colloids stabilized with polysaccharides. *Colloid Polym. Sci.* **278**, 491–501 (2000).
29. Usov, A. I. Polysaccharides of the red algae. in *Advances in Carbohydrate Chemistry and Biochemistry* 65 115–217 (Academic Press Inc., 2011).
30. dos Santos, M. A. & Grenha, A. Polysaccharide Nanoparticles for Protein and Peptide Delivery: Exploring Less-Known Materials. in *Advances in Protein Chemistry and Structural Biology* 98 223–261 (Academic Press Inc., 2015).
31. Liew, J. W. Y., Loh, K. S., Ahmad, A., Lim, K. L. & Wan Daud, W. R. Synthesis and characterization of modified κ-carrageenan for enhanced proton conductivity as polymer electrolyte membrane. *PLoS One* **12**, e0185313 (2017).
32. Mangione, M. R., Giacomazza, D., Bulone, D., Martorana, V. & San Biagio, P. L. Thermoreversible gelation of κ-Carrageenan: Relation between conformational transition and aggregation. *Biophys. Chem.* **104**, 95–105 (2003).
33. Platzman, I., Brener, R., Haick, H. & Tannenbaum, R. Oxidation of polycrystalline copper thin films at ambient conditions. *J. Phys. Chem. C.* **112**, 1101–1108 (2008).

34. Choudhary, S. et al. Oxidation mechanism of thin Cu films: A gateway towards the formation of single oxide phase. *AIP Adv.* **8**, 055114 (2018).
35. Gattinoni, C. & Michaelides, A. Atomistic details of oxide surfaces and surface oxidation: the example of copper and its oxides. *Surf. Sci. Rep.* **70**, 424–447 (2015).
36. Tye, Y. Y., Abdul Khalil H. P. S., Kok, C. Y. & Saurabh, C. K. Preparation and characterization of modified and unmodified carrageenan based films. in *IOP Conference Series: Materials Science and Engineering* 368 012020 (Institute of Physics Publishing, 2018).
37. Lefez, B., Kartouni, K., Lenglet, M., Rönnow, D. & Ribbing, C. G. Application of reflectance spectrophotometry to the study of copper (I) oxides (Cu2O and Cu3O2) on metallic substrate. *Surf. Interface Anal.* **22**, 451–455 (1994).
38. Biesinger, M. C. Advanced analysis of copper X-ray photoelectron spectra. *Surf. Interface Anal.* **49**, 1325–1334 (2017).
39. Berton, S. B. R. et al. Properties of a commercial κ-carrageenan food ingredient and its durable superabsorbent hydrogels. *Carbohydr. Res.* **487**, 107883 (2020).
40. Li, L. et al. FeS2/carbon hybrids on carbon cloth: A highly efficient and stable counter electrode for dye-sensitized solar cells. *Sustain. Energy Fuels* **3**, 1749–1756 (2019).
41. Zhou, G. et al. Oxygen bridges between nio nanosheets and graphene for improvement of lithium storage. *ACS Nano* **6**, 3214–3223 (2012).
42. Chen, X. et al. Green Synthesis of Gold Nanoparticles Using Carrageenan Oligosaccharide and Their In Vitro Antitumor Activity. *Mar. Drugs* **16**, 277 (2018).
43. Gün Gök, Z., Karayel, M. & Yiğitoğlu, M. Synthesis of carrageenan coated silver nanoparticles by an easy green method and their characterization and antimicrobial activities. *Res. Chem. Intermed.* **47**, 1843–1864 (2021).
44. Miccoli, I., Edler, F., Pfnür, H. & Tegenkamp, C. The 100th anniversary of the four-point probe technique: The role of probe geometries in isotropic and anisotropic systems. *J. Phys. Condens. Matter* **27**, 223201 (2015).
45. Joo, S. J., Hwang, H. J. & Kim, H. S. Highly conductive copper nano/microparticles ink via flash light sintering for printed electronics. *Nanotechnology* **25**, 265601 (2014).
46. Amert, A. K., Oh, D. H. & Kim, N. S. A simulation and experimental study on packing of nanoinks to attain better conductivity. in *Journal of Applied Physics* 108 102806 (American Institute of PhysicsAIP, 2010).
47. Woo, K., Kim, D., Kim, J. S., Lim, S. & Moon, J. Ink-jet printing of Cu-Ag-based highly conductive tracks on a transparent substrate. *Langmuir* **25**, 429–433 (2009).
48. Bakonyi, I. Accounting for the resistivity contribution of grain boundaries in metals: critical analysis of reported experimental and theoretical data for Ni and Cu. *Eur. Phys. J.* **136**, 410 (2021).
49. Kittel, C. *Introduction to Solid State Physics Charles Kittel*. 8 (2005).
50. Hill, R. M. Electrical conduction in ultra thin metal films I. Theoretical. *Proc. R. Soc. Lond. A. Math. Phys. Sci.* **309**, 377–395 (1969).
51. Sheng, P., Abeles, B. & Arie, Y. Hopping conductivity in granular metals. *Phys. Rev. Lett.* **31**, 44–47 (1973).
52. Dellinger, J. H. The temperature coefficient of resistance of copper. *J. Frankl. Inst.* **170**, 213–216 (1910).
53. Warkusz, F. The size effect and the temperature coefficient of resistance in thin films. *J. Phys. D: Appl. Phys.* **11**, 689 (1978).
54. Belser, R. B. & Hicklin, W. H. Temperature Coefficients of Resistance of Metallic Films in the Temperature Range 25° to 600 °C. *J. Appl. Phys.* **30**, 313–322 (1959).
55. Gall, D. The search for the most conductive metal for narrow interconnect lines. *J. Appl. Phys.* **127**, 50901 (2020).
56. Zeng, H. et al. Grain size-dependent electrical resistivity of bulk nanocrystalline Gd metals. *Prog. Nat. Sci. Mater. Int.* **23**, 18–22 (2013).
57. Gao, Y. et al. Novel copper particle paste with self-reduction and self-protection characteristics for die attachment of power semiconductor under a nitrogen atmosphere. *Mater. Des.* **160**, 1265–1272 (2018).
58. Jacob, U., Vancea, J. & Hoffmann, H. Surface-roughness contributions to the electrical resistivity of polycrystalline metal films. *Phys. Rev. B* **41**, 11852 (1990).
59. West, P. R. et al. Searching for better plasmonic materials. *Laser Photonics Rev.* **4**, 795–808 (2010).
60. Pereira, H. J. et al. Fabrication of Copper Window Electrodes with ≈10 8 Apertures cm −2 for Organic Photovoltaics. *Adv. Funct. Mater.* **28**, 1802893 (2018).
61. Bellchambers, P. et al. Elucidating the exceptional passivation effect of 0.8 nm evaporated aluminium on transparent copper films. *Front. Mater.* **5**, 71 (2018).
62. Brunetti, F. et al. Printed Solar Cells and Energy Storage Devices on Paper Substrates. *Adv. Funct. Mater.* **29**, 1806798 (2019).
63. Yao, B. et al. Paper-Based Electrodes for Flexible Energy Storage Devices. *Adv. Sci.* **4**, 1700107 (2017).
64. LaDou, J. Printed circuit board industry. *Int. J. Hyg. Environ. Health* **209**, 211–219 (2006).
65. Mirvakili, S. M., Broderick, K. & Langer, R. S. A New Approach for Microfabrication of Printed Circuit Boards with Ultrafine Traces. *ACS Appl. Mater. Interfaces* **11**, 35376–35381 (2019).
66. Komolafe, A. et al. Integrating Flexible Filament Circuits for E-Textile Applications. *Adv. Mater. Technol.* **4**, 1900176 (2019).
67. Kim, D. J. et al. Indium-free, highly transparent, flexible Cu2O/Cu/Cu2O mesh electrodes for flexible touch screen panels. *Sci. Rep.* **5**, 1–10 (2015). *2015 51*.
68. Wang, B. Y., Yoo, T. H., Song, Y. W., Lim, D. S. & Oh, Y. J. Cu ion ink for a flexible substrate and highly conductive patterning by intensive pulsed light sintering. *ACS Appl. Mater. Interfaces* **5**, 4113–4119 (2013).
69. Saleh, R., Barth, M., Eberhardt, W. & Zimmermann, A. Bending Setups for Reliability Investigation of Flexible Electronics. *Micromachines* **12**, 1–22 (2021).
70. Yang, Y., Huang, Q., Payne, G. F., Sun, R. & Wang, X. A highly conductive, pliable and foldable Cu/cellulose paper electrode enabled by controlled deposition of copper nanoparticles. *Nanoscale* **11**, 725–732 (2019).
71. Schreck, M., Deshmukh, R., Tervoort, E. & Niederberger, M. Impregnation of Cellulose Fibers with Copper Colloids and Their Processing into Electrically Conductive Paper. *Chem. Mater.* **34**, 43–52 (2022).
72. Pinto, R. J. B. et al. Highly Electroconductive Nanopapers Based on Nanocellulose and Copper Nanowires: A New Generation of Flexible and Sustainable Electrical Materials. *ACS Appl. Mater. Interfaces* **12**, 34208–34216 (2020).
73. De Vos, M., Torah, R., Beeby, S. & Tudor, J. Functional Electronic Screen-printing – Electroluminescent Lamps on Fabric. *Procedia Eng.* **87**, 1513–1516 (2014).
74. De Vos, M., Torah, R. & Tudor, J. Dispenser printed electroluminescent lamps on textiles for smart fabric applications. *Smart Mater. Struct.* **25**, 045016 (2016).
75. Daerr, A. & Mogne, A. Pendent_Drop: An ImageJ Plugin to Measure the Surface Tension from an Image of a Pendent Drop. *J. Open Res. Softw.* **4**, 3 (2016).

Acknowledgements

We thank the Propulsion Futures Beacon of Excellence at the University of Nottingham for funding and facilities. We thank the Schools of Chemistry and Physics, the Nanoscale and Microscale Research Centre (nmRC) of University of Nottingham and School of Electronics and Computer Science of University of Southampton for research facilities. The authors sincerely acknowledge, Dr. Craig Stoppiello and Dr. Long Jiang (XPS), Dr. Michael Fay (TEM), Dr. Tong Liu (elemental analysis) and Dr. Zhongnan Duan (MALDI-

TOF-MS) for their support. HJP thanks University of Southampton for the award of an Anniversary Fellowship and funding.

Author contributions

H.J.P. conceived the study, designed and conducted experiments, analysed and interpreted the data and wrote the first draft of the article. O.M. supported in the design of experiments in relation to determining electrical properties of Cu films. O.M., D.B.A. and G.N.N. provided resources and supported in analysis and interpretation of data. All authors reviewed, edited, and approved the final manuscript.

Competing interests

The authors declare no competing interests.

Additional information

Supplementary information The online version contains supplementary material available at https://doi.org/10.1038/s41528-024-00331-1.

Correspondence and requests for materials should be addressed to H. Jessica Pereira.